Selective Oxidation of Short-Chain Alcohols on Spinel $CoFe_2O_4$ (001) Surfaces: Mechanistic Insights from DFT

Arjeta Rushiti* and Christof Hättig*

Lehrstuhl für Theoretische Chemie, Ruhr-Universität Bochum, 44801 Bochum, Germany

E-mail: Arjeta.Rushiti@rub.de; christof.haettig@rub.de

Abstract

The selective oxidation of short-chain alcohols is a key transformation in green chemistry, providing sustainable routes to aldehydes and ketones for industrial applications. In this study, we present a mechanistic density functional theory (DFT) investigation of alcohol oxidation on spinel $CoFe_2O_4$ (001) surfaces. Using an embedded cluster model, we compare the reactivity of the A- and B-layer terminations, focusing on the role of monoatomic reactive oxygen species (ROS) and lattice oxygen in the Langmuir–Hinshelwood and Mars–van Krevelen pathways. Adsorption energies, deprotonation barriers, and product stabilization are evaluated for methanol, ethanol, and 2-propanol, highlighting the interplay of surface cation identity and local coordination environment. Our results reveal that Fe−O oxyl species on the A-layer provide thermodynamically and kinetically favorable pathways, while the B-layer favors lattice oxygen participation with lower barriers in the second deprotonation step. The findings rationalize experimental observations of superior activity associated with Co^{3+}-rich environments and offer molecular-level insights into tailoring spinel oxide catalysts for selective alcohol oxidation.

Introduction

Selective oxidation of alcohols to aldehydes or ketones is among the most fundamental organic reactions and representatives of green chemistry.[1,2] These oxygenated products are widely used as solvents, polymer precursors, high value-added components in cosmetics, and intermediates of dyes as well as pharmaceuticals, agrochemicals, and lubricants.[3–6]

The synthesis of aldehydes and ketones via catalytic alcohol oxidation has been demonstrated for a range of materials including noble and non-noble metals, metal oxides, and composites of the two. However, while metal catalysts such as Pt, Pd, Au, or Ru are usually quite efficient in the partial oxidation of aromatic and activated allylic alcohols, they are less selective for the oxidation of aliphatic and, especially, primary alcohols.[1,7] In addition,

because of the limited availability, high costs, and high sintering rates of precious metals, it is desirable to rely on more economical solutions based on earth-abundant metals. To this end, transition metal oxides of the spinel type with general formula AB_2O_4 are promising alternatives. In particular, spinels in the form of ferrites[8,9] and cobaltites[10,11] have shown high catalytic activity in electrocatalysis[12–15] as well as in the catalytic combustion of CO[16–18] and the decomposition reactions of several hydrocarbons[19–22] .

The enhanced catalytic performance of spinels stems from the ability to accommodate a wide range of metal cations and oxidation states in different coordination environments, both in the bulk and at the surface. For instance, in bulk cobalt ferrite, $CoFe_2O_4$ (CFO), Fe^{3+} cations are distributed over 1/8 of the tetrahedral interstices (T_d or A-sites) in the face-centered cubic lattice, whereas 1/2 of the octahedral interstices (O_h or B-sites) are occupied by Co^{2+} and Fe^{3+}. The redox properties of CFO can then easily be tuned by manipulating the distribution of different cations on T_d or O_h positions as well as by cation exchange, while the crystal structure remains stable.

Several experimental studies[23–26] so far have observed the synergistic effects between Fe and Co in catalytic reactions of selective alcohol oxidation on spinels, both in the gas and in the liquid phase.[27–30] To give some examples, Waffel et al.[27] investigated, in a comparative approach, the partial oxidation of aromatic alcohols and olefins over a systematic series of $Co_{3-x}Fe_xO_4$ catalysts in the liquid phase, with O_2 and *tert*-butyl hydroperoxide (TBHP) as oxidizing agents. This comparison revealed that Fe substitution in the spinel structure is beneficial only when TBHP is used. In another contribution, Falk et al.[28] applied a series of $Co_{1+x}Fe_{2-x}O_4$ spinel nanowires in the aerobic oxidation of 2-propanol to systematically study the influence of exposed Fe and Co cations on the catalytic properties, with and without water vapor co-feeding. They report acetone as the main product at temperatures below 180 ° C and attribute the catalytic activity to ensembles of at least six coordinatively unsaturated Co^{3+} ions.

In terms of reaction pathways, Anke et al.[31] found that 2-propanol is oxidatively dehy-

drogenated to acetone and H_2O over unsupported Co_3O_4 nanoparticles, reaching almost full conversion with 100 % selectivity at 430 K. The results could be fitted well using the Mars-van Kreveln (MvK) mechanism[32] at the expense of lattice oxygen, although a non-negligible contribution of the Langmuir-Hinshelwood mechanism[33,34] involving adsorbed atomic oxygen was also observed. In fact, complementary periodic density functional theory (DFT) calculations showed a thermodynamic preference for the latter mechanism and identified the 5-fold coordinated Co^{3+} species as active sites. Similar findings were encountered for CFO nanoparticles[29] although with a lower catalytic activity, which based on X-ray photoelectron spectroscopy (XPS) was attributed to the presence of significantly less reactive Co^{2+} species. The superior catalytic activity of the Co^{3+} cations relative to Co^{2+} has also been observed by Lv et al.[35] who performed DFT calculations to study methanol oxidation on the (110) and (111) surfaces of Co_3O_4. Lv et al.[35] report activation energies which are overall lower on the (110) surface exposing Co^{3+} species than on (111) exposing Co^{2+}, while also demonstrating the implications of lattice oxygen in the proposed MvK redox cycles.

To contribute to this evolving field relating the interplay of composition, structure, and reactivity in Fe and Co-based spinels oxides for the selective oxidation of alcohols, in recent publications, we theoretically addressed the influence of surface reduction,[36] formation of reactive oxygen species (ROS),[37] and adsorption mechanism of short-chain alcohols (methanol, ethanol, and 2-propanol) on CFO surfaces.[38] Of the two most abundant facets in CFO nanoparticles, (001) and (111),[39] we focused on the (001) termination with significantly lower overpotential for water oxidation relative to (111), and a better agreement to the experimental value.[25]

The present work extends and complements our preliminary studies on CFO (001) surfaces and reports a detailed mechanistic DFT investigation on the partial oxidation of short-chain alcohols (methanol, ethanol, and 2-propanol) with ROS in the gas phase as an industrially feasible and environmentally benign protocol. We employ an embedded cluster approach to model two surfaces of the (001) terminations, the so-called A and B layers, the

atomic arrangement of which differs in the presence of the Fe monolayer (2-fold coordinated).

By taking into account the experimental findings on Co_3O_4 and CFO nanoparticles,[29,31] we limit the computational study only on the oxidative dehydrogenation pathways following the Langmuir-Hinshelwood and the MvK mechanisms. Furthermore, in view of the fact that O_2 temperature programmed desorption (TPD) experiments excluded the presence of molecular oxygen species on CFO nanoparticles,[29] only the role of the monoatomic ROS and lattice oxygen is explored. Theoretical studies considering the Eley-Rideal mechanism are set aside due to the high energy costs of pre-adsorbed atomic oxygen species reported in our previous study.[37]

Computational Methods

All DFT calculations were carried out in combination with the periodic electrostatic embedded cluster model (PEECM)[40] as implemented in the TURBOMOLE V7.4 program package.[41] The strongly correlated electrons in CFO are accounted for at the PBE0[42]/ def2-SVP[43] level, by applying the resolution of identity approximation for the electronic Coulomb interaction term, with auxiliary basis sets[44] optimized for the corresponding orbital basis sets.

Finite-sized clusters modelling the (001)-A and B surfaces of CFO with different metal active sites as close to the center as possible are presented in Figure 1 and range from 75 to 135 atoms. They are treated quantum mechanically in the same setup which was validated

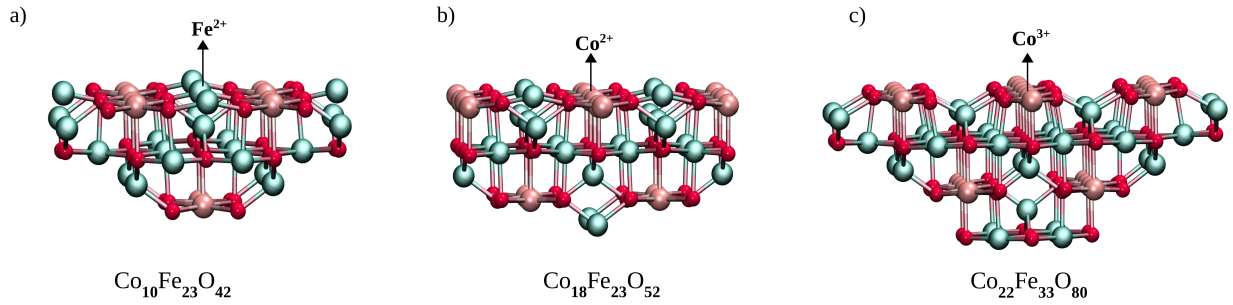


Figure 1: The cluster structures built symmetrically around the a)Fe b) Co^{Af} and Co^{Ah} sites at the A-layer and c) Co^{B} and oxygen vacancy at the B-layer of CFO (001) surfaces.

in our previous study.[37]

To obtain optimized geometries of equilibrium and transition state structures only the geometry of the most inner part of the quantum cluster is allowed to relax and adjust to the method and the introduced defects and/or adsorbates. An initial guess for the transition states is obtained by using the chain-of-state method implemented in the woelfling module[45] of TURBOMOLE, and the transitions states are further refined using the trust-region image minimization (TRIM) algorithm.[46] For the convergence criteria, the *m5* DFT grid is used with thresholds of 1×10^{-8} and 1×10^{-3} for the total energy and the maximum norm of the Cartesian energy gradient, respectively. For the self-consistent field (SCF) part, the augmented Roothaan–Hall method[47] for solving the Kohn–Sham equations is employed.

Adsorption energies are determined as the energy differences between the cluster − adsorbate complexes and fully separated structures, with zero-point vibrational energy contributions calculated within the harmonic approximation. The energies of the monoatomic ROS are determined with respect to half of the energy of molecular O_2. The Hessian matrix and the dipole gradients for the vibrational frequency calculations are computed by considering the derivatives of the quadrature weights and a numerical differentiation of the gradients, with a stepwidth of 0.02 a.u. for the Cartesian coordinate displacements.

Exceptions are the calculations for 2-propanol for which the *m3* DFT grid is used with thresholds of 1×10^{-6} and 1×10^{-3} for the total energy and the maximum norm of the Cartesian energy gradient, respectively, and the energies are not corrected yet for the zero-point vibrational energy (ZPVE) contribution.

Results

The reaction pathways and product selectivity observed during the oxidation of alcohols over heterogeneous catalysts is quite diverse and strongly dependent on the identity of the reaction site and the detailed molecular structure of the reactants. At CFO (001) surface

termination adsorbants can bind on several sites: the two fold-coordinated $Fe^{+2}(T_d)$ and five-fold coordinated $Co^{+2}(O_h)$ at the A layer and the five-fold coordinated $Co^{+3}(O_h)$ at the B layer. In addition we considered the most stable vacancy at B layer, i.e. the O1 vacancy, as an active site due to its implication in the MvK mechanism. To differentiate between the active Co in the A and B layer, respectively, we use the Co^A and Co^B naming convention. The effect of surface relaxation on molecule adsorption was studied using cluster $Co_{18}Fe_{23}O_{52}$ (Figure 1b) which represents a surface model of the A layer with $Co^{+2}(O_h)$ surface sites of different degrees of flexibility in their coordination structure, namely, the 'hindered' Co cations (hereafter denoted as Co^{Ah}) compromised (to some extent) by the reduced bond lengths and the close proximity of the additional monolayer of Fe and the 'free' Co (hereafter denoted as Co^{Af}) which remain more accessible as the Fe cations relax away.[25]

For the mechanistic investigation we focused the following plausible steps:

1. Adsorption of reactants: alcohols and ROS
2. First deprotonation step: O−H bond cleavage
3. Second deprotonation step: C−H activation
4. Desorption of products: aldehyde and water

A layer

At the A-layer, we have considered the Langmuir-Hinshelwood oxidative dehydrogenation mechanism such that the alcohol molecules and the monoatomic ROS co-adsorb at metal sites adjacent to each other. In total, we distinguish four cases denoted with roman numbers I-IV. In case I, monoatomic oxygen species adsorb on the Co^{Ah} site whereas the alcohol molecule adsorbs on Co^{Af}. The reverse adsorption case is denoted with II. The Fe–Co^A cation pair is considered in case III, in which the atomic oxygen adsorbs on the Fe site whereas the alcohol

molecule adsorbs on the closest cobalt, i.e., Co^{Ah}. The reverse adsorption case is denoted with IV.

Case I. The results which correspond to this case are presented in Figure 2. In the adsorption step, the alcohol molecule adsorbs with its O-atom oriented such that the O−H functional group forms a hydrogen bond (H-bond) with the ROS, with bond distances of 1.64, 1.65, and 1.66 Å for methanol, ethanol, and 2-propanol, respectively. Adsorption energies associated with such an interaction become more negative in the following order methanol > ethanol > 2-propanol. (However, we note once again that the results on 2-propanol are not corrected for the ZPVE and are calculated with lower threshold criteria.) The Co−O_{ROS} distances are 1.84 Å, whereas the Co-$O_{alcohol}$ distances are 2.10 Å for methanol and ethanol, and slightly larger (2.12 Å) for 2-propanol.

As previously mentioned, for the 1^{st} deprotonation step, we considered the O−H bond scission. The calculated energy barriers for this step are 17.8 and 17.5 kJ/mol for methanol and ethanol, respectively. Once the H is tranfered to the ROS, the OH group relaxes in a bridging position between the hosting Co site and the 2-fold coordinated Fe(T_d) from the A monolayer, with distances of 2.05 and 2.06 Å. The Co-$O_{alcohol}$ distance shrinks by 0.03 Å from the adsorption step (1.81 Å), indicating a stronger interaction of the alkoxy group with the metal center.

For the 2^{nd} deprotonation, we considered the O-assisted activation of C−H via the closest oxygen from the lattice as well as via the OH group formed in the previous step by a transfer of the H (from the O−H bond cleavage) to the reactive adoxygen species. Of these two possibilities, direct transfer of H to OH forming water and an aldehyde/ketone, resulted in a configuration which is overall more negative in energy, however, the transition states (energy barriers) for such a process still need to be determined. The C−H activation through lattice oxygen has to surpass an energy barrier of 30.8 kJ/mol for methanol.

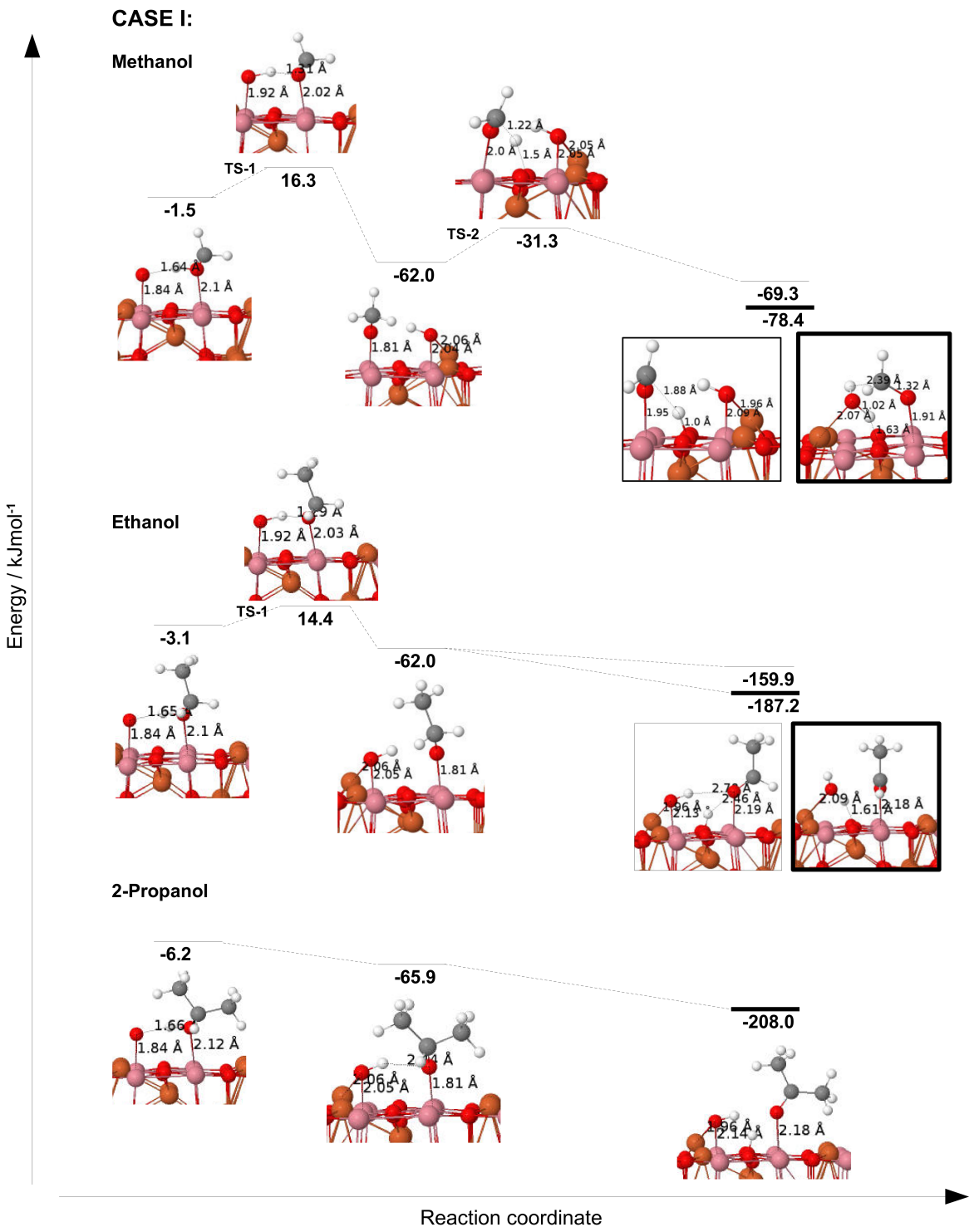


Figure 2: Plausible pathway following the Langmuir-Hinshelwood mechanism for the selective oxidation of short-chain alcohols (methanol, ethanol, and 2-propanol) at the A layer when the alcohol molecule adsorbs on top of Co^{Af} whereas the reactive adoxygen species adsorbs on top of the adjacent metal site, i.e., Co^{Ah}.

Case II. The results which correspond to this case are presented in Figure 3. In a similar manner as for case I, in the adsorption step the alcohol molecules adsorbs via the oxygen atom on top of the hosting Co site and, in addition, they form a H-bond with the ROS. An exception is the 2-propanol molecule which after optimization is transfered on top of the Fe site at the A monolayer. The bond distances for the H-bond are 1.64 and 1.65 Å for methanol and ethanol, respectively, identical to case I. Since in this scenario the ROS adsorbs on the 'free' Co and the acohol molecule adsorbs on the 'hindered' Co, the corresponding metal-O distances differ from case I, as follows: the Co$-$O$_{ROS}$ distance is 1.82 Å (by 0.02 Å shorter than that of O on top of Co^{Ah}) and the Co$-$O$_{alcohol}$ distance is 2.16 Å (by 0.06 Å larger than in the previous case).

The more positive adsorption energies associated with these structures indicate that case II is thermodynamically less favorable than case I. The same can be observed for the 1st deprotonation step as well, such that the structures in case II are by approx. 30 kJ/mol less favorable. By contrast, the activation energies for the O$-$H bond cleavage are significantly smaller, i.e., 6.6 and 6.3 kJ/mol for methanol and ethanol. In the final geometry of this elementary step, the metal-O interactions are stronger as indicated by the shorter bond distances.

In the following, C$-$H activation and transfer of H to lattice oxygen is associated with an energy barrier of 59.6 and 51.0 kJ/mol for methanol and ethanol, respectively. For methanol, this activation energy is larger than the one when H is transferred to the previously formed OH (34.5 kJ/mol). In addition, the local minimum associated with the latter is by 37.8 kJ/mol more negative in energy. For ethanol and the two possible local minima this difference in energy is 38.5 kJ/mol, whereas the corresponding energy barrier for the direct transfer of H to OH needs to be determined. The products in this step are more loosely bound to the hosting metal sites as indicated by the enlargement in the corresponding bond distances.

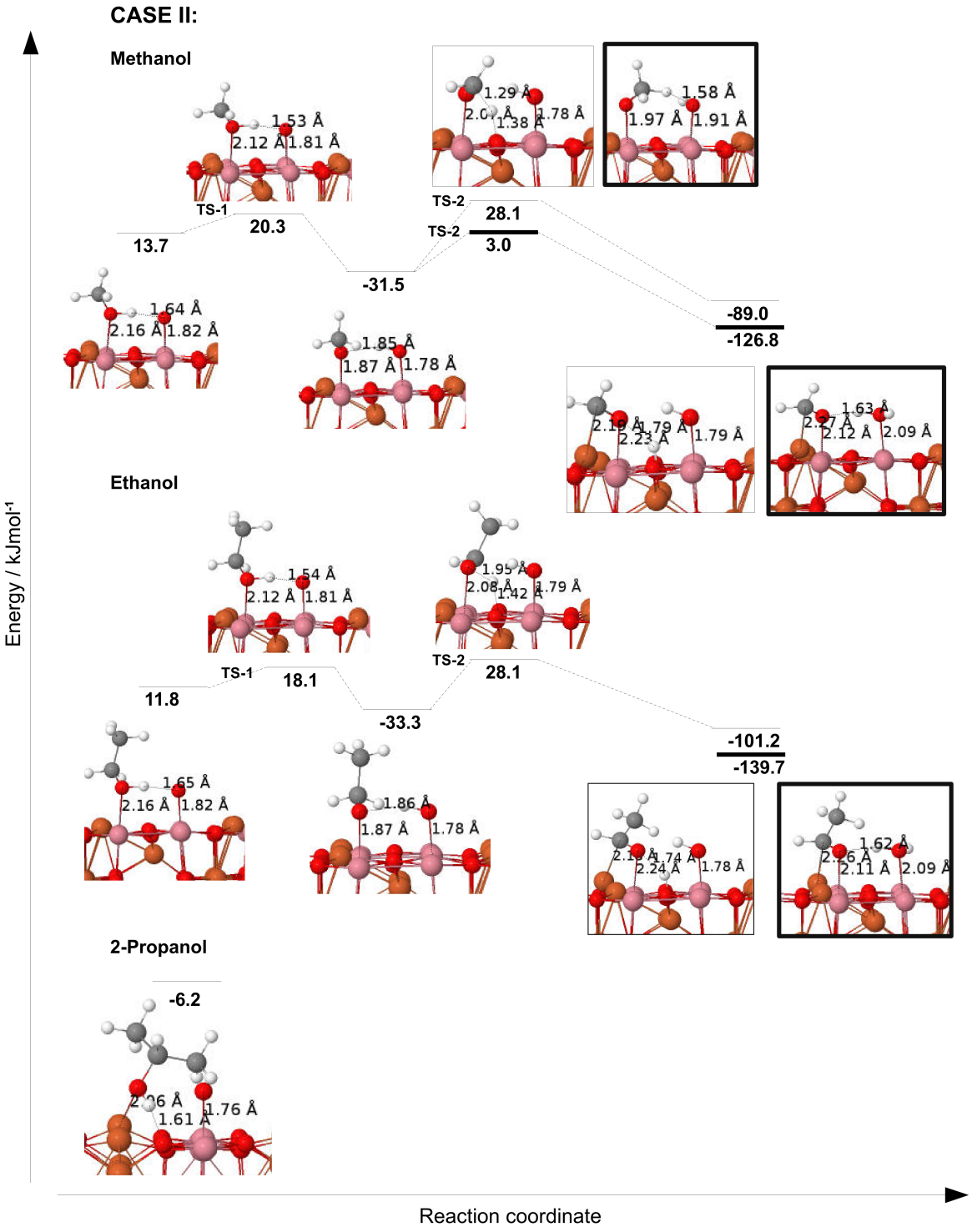


Figure 3: Plausible pathway following the Langmuir-Hinshelwood mechanism for the selective oxidation of short-chain alcohols (methanol, ethanol, and 2-propanol) at the A layer when the alcohol molecule adsorbs on top of Co^{Ah} whereas the reactive adoxygen species adsorbs on top of the adjacent metal site, i.e., Co^{Af}.

Case III. The results which correspond to this case are presented in Figure 4. A quick comparison of the energetic profile with the previous cases in Figure 2 and Figure 3 reveals that case III is both thermodynamically and kinetically more favorable. This because the local minima are located lower in energy, and the activation barriers for the $1st$ and 2^{nd} deprotonation steps are smaller. The O−H bond cleavage is an exothermic process with no apparent transition state as indicated by a barrierless woelfling-path for methanol, and a transition state which is lower in energy than the initial configuration for ethanol. The larger energetic stability of the structures in case III relative to cases I and II is related to the thermodynamic preference of the O adatom to reside on Fe sites; as reported in our previous paper on the activation of molecular O_2,[37] the Fe−O oxyl species are from 58.7 to 64.4 kJ/mol more stable than the Co−O oxyl species at the A layer.

For the 2^{nd} deprotonation step and the H transfer to lattice O, we distinguish two configurations depending on the geometry of the aldehyde. In one scenario the aldehyde is stabilized in η^2(C,O) configuration on top of two Co sites, whereas in the second scenario it is stabilized through the oxygen atom, but with elongated Co−O distance. The latter structure is energetically more favored.

Case IV. The results which correspond to this case are presented in Figure 5. Initially, the alcohols and the ROS adsorb on top of Fe and Co^{Ah}, respectively, with adsorption energies which are less favorable than in case III, yet, more negative than in cases I and II. Similarly, a H-bond is present between the OH group from the alcohol and the ROS, with bond lengths which are shorter than in the previous cases. Again, the energies become more negative in the following order: methanol > ethanol > 2-propanol.

The 1^{st} deprotonation step in methanol is associated with an energy barrier of 22.0 kJ/mol, whereas for ethanol and 2-propanol this barrier needs to be computed.

For the 2^{nd} deprotonation step, we considered three different final configurations. In two of them, the C−H hydrogen is transferred to the nearest oxygen from the lattice and the aldehyde is stabilized either on top of Fe via η^2(C,O) coordination or via η^1(O) coordination.

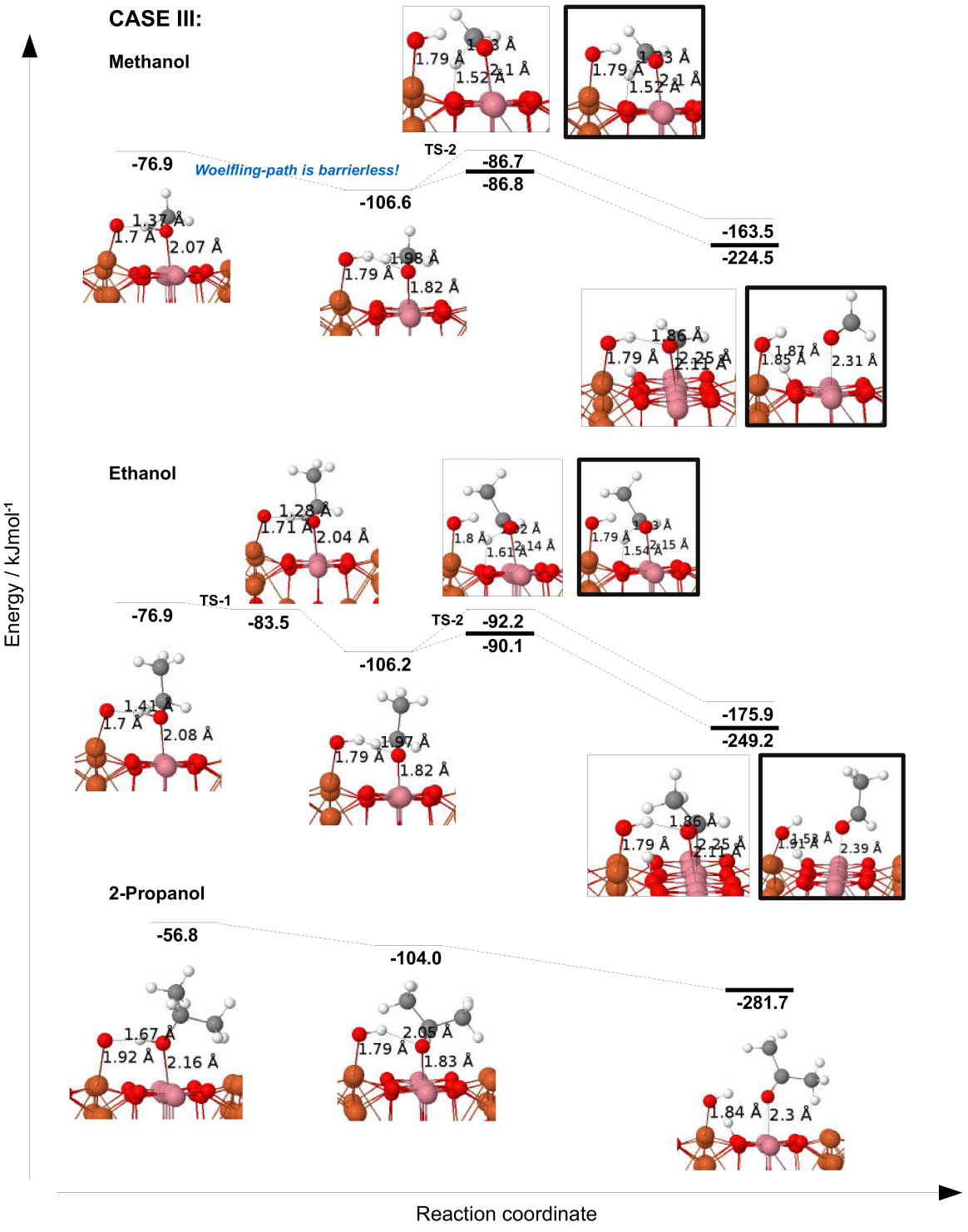


Figure 4: Plausible pathway following the Langmuir-Hinshelwood mechanism for the selective oxidation of short-chain alcohols (methanol, ethanol, and 2-propanol) at the A layer when the alcohol molecule adsorbs on top of Co^{Ah} whereas the reactive adoxygen species adsorbs on top of 2-fold coordinated Fe(T_d).

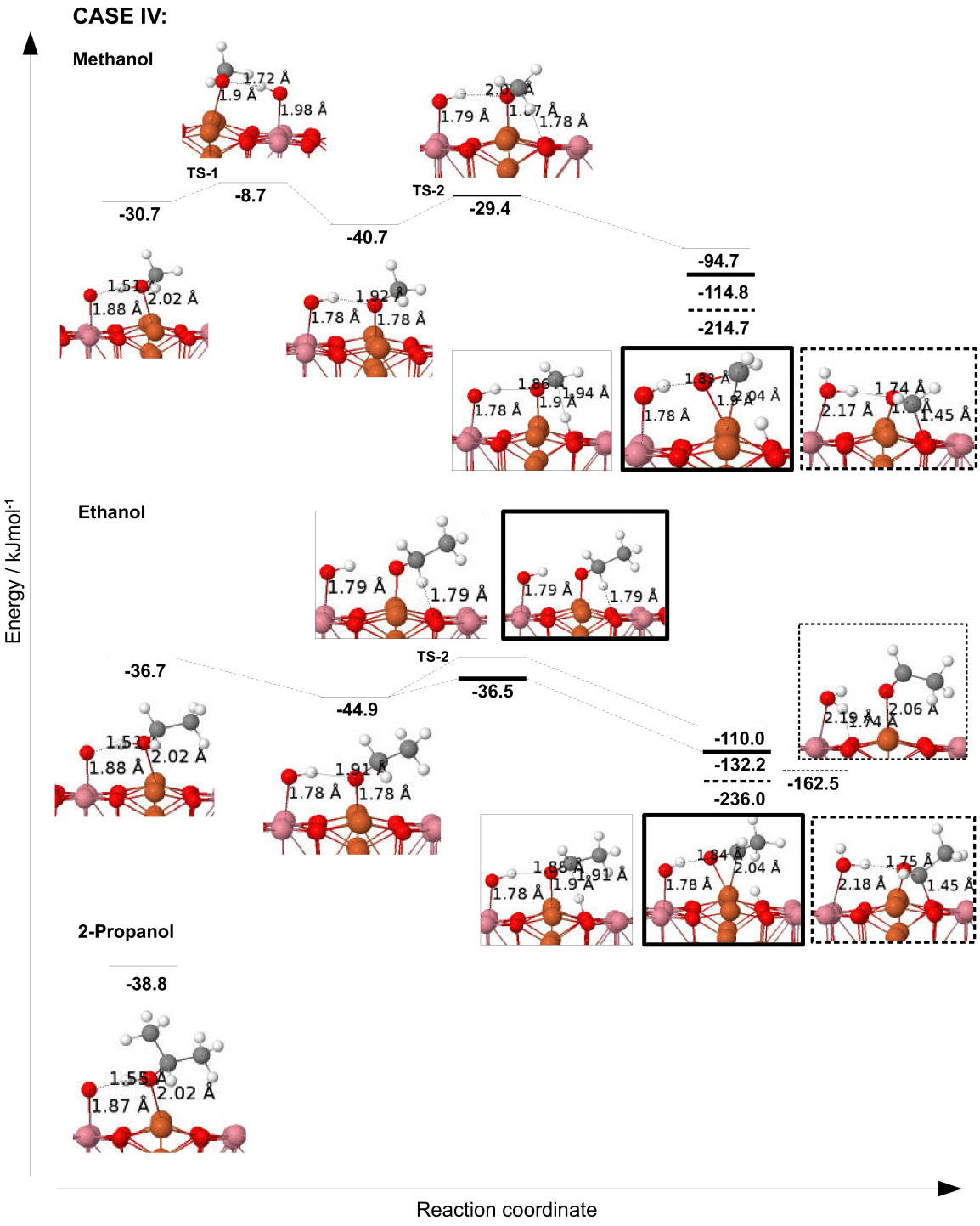


Figure 5: Plausible pathway following the Langmuir-Hinshelwood mechanism for the selective oxidation of short-chain alcohols (methanol, ethanol, and 2-propanol) at the A layer when the alcohol molecule adsorbs on top of the 2-fold coordinated Fe(T_d) whereas the reactive adoxygen species adsorbs on top of Co^{Ah}.

In the third configuration, the H is transferred to the OH group on top of Co^{Ah} (forming H_2O) and the aldehyde in stabilized in η^2(C,O) coordination between Fe and lattice oxygen. This is also the most stable geometry. For ethanol, we distinguish an additional fourth adsorption configuration such that water molecule on top of Co^{Ah} is H-bonded to lattice O, however, this geometry is less stable than the one where water remains H-bonded to the acetaldehyde.

B layer

At the B layer, we have considered both the Langmuir-Hinshelwood oxidative dehydrogenation mechanism as well as the Mars-van Krevelen mechanism at the expense of lattice oxygen of the O1 type (the most stable vacancy).

Focusing first on the Langmuir-Hinshelwood pathway the results of which are presented in Figure 6, one can see that the activation barriers associated with the first deprotonation step are higher than for any of the Langmuir-Hinshelwood cases at the A-layer; these barriers are 44.4 and 44.3 kJ/mol for methanol and ethanol, whereas at the A-layer they fall within the 0.0 - 22.0 kJ/mol range. The initial and final configurations of this elementary step are also close in energy: for methanol the energy difference is 1.4 kJ/mol, while for ethanol the difference is slightly larger, 2.8 kJ/mol.

For the 2^{nd} deprotonation, once again we considered the direct transfer of H to the OH group formed in the previous step as well as the H transfer to the closest O from the lattice. The former is more stable, however, the transition states and energy barriers that correspond to this process need to be calculated. On the other hand, the H transfer to the lattice has to surpass energy barriers of 23.9 and 13.8 kJ/mol for methanol and ethanol, respectively.

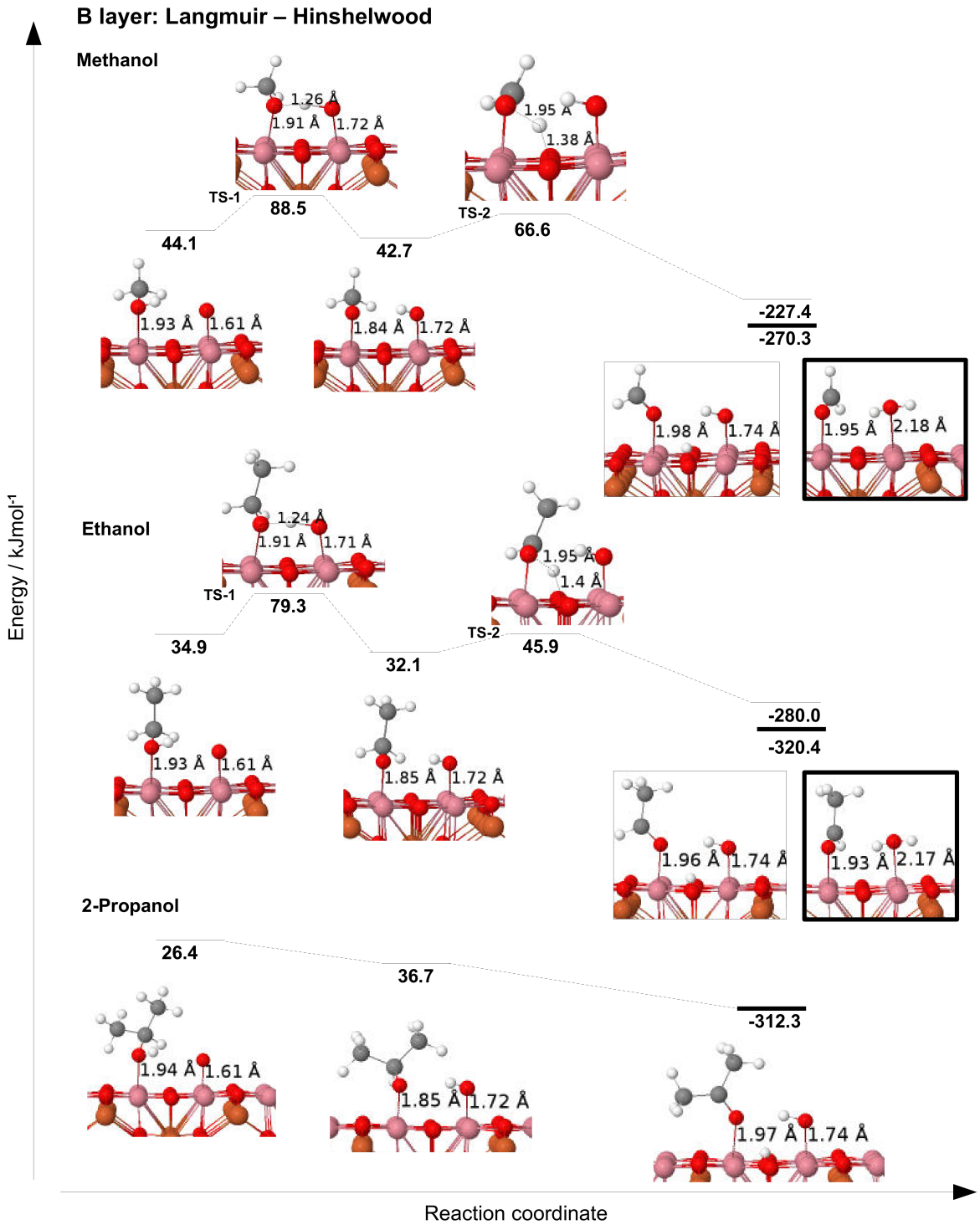


Figure 6: Plausible pathway following the Langmuir-Hinshelwood mechanism for the selective oxidation of short-chain alcohols (methanol, ethanol, and 2-propanol) at the B layer when the alcohol molecule and the reactive adoxygen species adsorbs on top of adjacent Co sites.

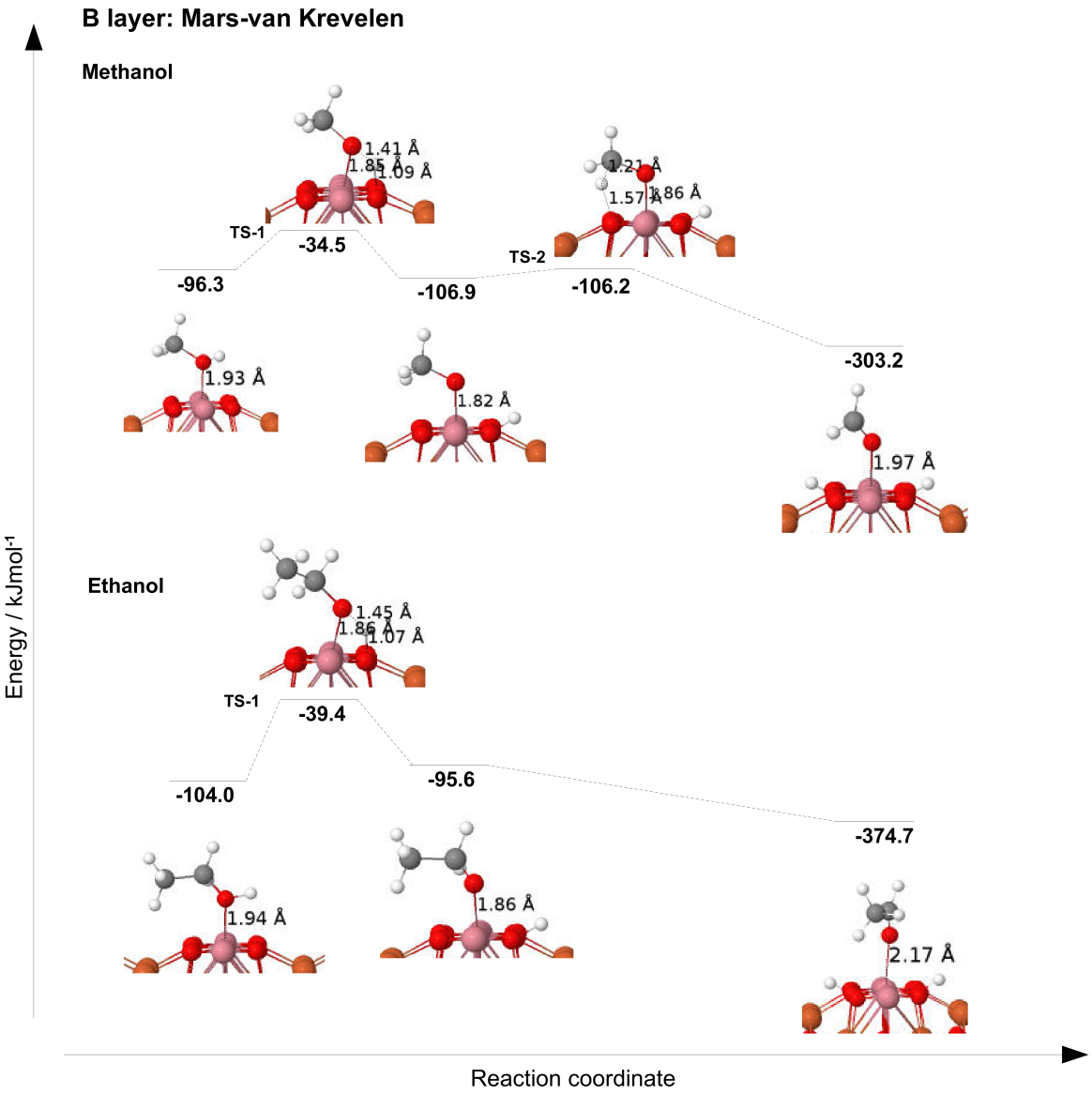


Figure 7: Plausible pathway following the Marc-van Krevelen mechanism for the selective oxidation of short-chain alcohols (methanol, ethanol, and 2-propanol) at the B layer at the expense of the lattice oxygen of the O1 type.

Turning next to the Mars-van Krevelen mechanism in Figure 7, one can see that the intermediate structures are located lower in the energy profile in comparison to the Langmuir-Hinshelwood case. The activation energy for the O−H scission, however, is largest (61.8 and 64.6 kJ/mol for methanol and ethanol). For the 2^{nd} deprotonation, the activation energy is only 0.8 kJ/mol (methanol) as H is transferred at the lattice O1.

Outlook

First, all missing transition states need to be calculated. For a more comprehensive description on the nature of the active sites, intrinsic bond orbital and charge analysis need to be performed. Furthermore, the desorption of products need to be considered. So far, no woelfing-path has been performed for the desorption of the products. There are a couple of possibilities:

- for the structures where in the 2^{nd} deprotonation step the H is transfer to lattice one can consider the desorption of the aldehyde first and then association of water and consequently its desorption. Alternatively, one could consider the association of water molecule as long as the aldehyde still binds to the surface, followed by the desorption of the two products. Also, separate and sequential desorption of the two products can be considered for the latter.

- for the structures in the 2^{nd} deprotonation step where the H is transfer to OH one can consider the simultaneous and also the sequential desorption of the products.

Acknowledgement

This work was funded by the Deutsche Forschungsgemeinschaft (DFG, German Research Foundation, project number 388390466–TRR 247, Project A5).

References

(1) Guo, Z.; Liu, B.; Zhang, Q.; Deng, W.; Wang, Y.; Yang, Y. Recent advances in heterogeneous selective oxidation catalysis for sustainable chemistry. *Chem. Soc. Rev.* **2014**, *43*, 3480–3524.

(2) Davis, S. E.; Ide, M. S.; Davis, R. J. Selective oxidation of alcohols and aldehydes over supported metal nanoparticles. *Green Chem.* **2013**, *15*, 17–45.

(3) Matsumoto, T.; Ueno, M.; Wang, N.; Kobayashi, S. Recent advances in immobilized metal catalysts for environmentally benign oxidation of alcohols. *Chem. Asian J.* **2008**, *3*, 196–214.

(4) Chen, Y.; Bai, L.; Zhou, C.; Lee, J.-M.; Yang, Y. Palladium-catalyzed aerobic oxidation of 1-phenylethanol with an ionic liquid additive. *Chem. Commun.* **2011**, *47*, 6452–6454.

(5) Chen, Y.; Lim, H.; Tang, Q.; Gao, Y.; Sun, T.; Yan, Q.; Yang, Y. Solvent-free aerobic oxidation of benzyl alcohol over Pd monometallic and Au–Pd bimetallic catalysts supported on SBA-16 mesoporous molecular sieves. *Appl. Catal. A: Gen.* **2010**, *380*, 55–65.

(6) Liu, F.; Wang, H.; Sapi, A.; Tatsumi, H.; Zherebetskyy, D.; Han, H.-L.; Carl, L. M.; Somorjai, G. A. Molecular orientations change reaction kinetics and mechanism: A review on catalytic alcohol oxidation in gas phase and liquid phase on size-controlled Pt nanoparticles. *Catalysts* **2018**, *8*, 226.

(7) Zhao, J.; Hernández, W. Y.; Zhou, W.; Yang, Y.; Vovk, E.; Capron, M.; Ordomsky, V.; others Selective oxidation of alcohols to carbonyl compounds over small size colloidal Ru nanoparticles. *ChemCatChem* **2020**, 238–247.

(8) Zhu, H.; Zhang, S.; Huang, Y.-X.; Wu, L.; Sun, S. Monodisperse M x $Fe_{3-x}O_4$ (M= Fe, Cu, Co, Mn) nanoparticles and their electrocatalysis for oxygen reduction reaction. *Nano Lett.* **2013**, *13*, 2947–2951.

(9) Indra, A.; Menezes, P. W.; Sahraie, N. R.; Bergmann, A.; Das, C.; Tallarida, M.; Schmeißer, D.; Strasser, P.; Driess, M. Unification of catalytic water oxidation and oxygen reduction reactions: amorphous beat crystalline cobalt iron oxides. *J. Am. Chem. Soc.* **2014**, *136*, 17530–17536.

(10) Kim, T. W.; Woo, M. A.; Regis, M.; Choi, K.-S. Electrochemical synthesis of spinel type $ZnCo_2O_4$ electrodes for use as oxygen evolution reaction catalysts. *J. Phys. Chem. Lett.* **2014**, *5*, 2370–2374.

(11) Zhu, C.; Wen, D.; Leubner, S.; Oschatz, M.; Liu, W.; Holzschuh, M.; Simon, F.; Kaskel, S.; Eychmüller, A. Nickel cobalt oxide hollow nanosponges as advanced electrocatalysts for the oxygen evolution reaction. *Chem. Commun.* **2015**, *51*, 7851–7854.

(12) Trotochaud, L.; Young, S. L.; Ranney, J. K.; Boettcher, S. W. Nickel–iron oxyhydroxide oxygen-evolution electrocatalysts: the role of intentional and incidental iron incorporation. *J. Am. Chem. Soc.* **2014**, *136*, 6744–6753.

(13) Cheng, F.; Shen, J.; Peng, B.; Pan, Y.; Tao, Z.; Chen, J. Rapid room-temperature synthesis of nanocrystalline spinels as oxygen reduction and evolution electrocatalysts. *Nature Chem.* **2011**, *3*, 79–84.

(14) Hamdani, M.; Singh, R.; Chartier, P. Co_3O_4 and Co-based spinel oxides bifunctional oxygen electrodes. *Int. J. Electrochem. Sci* **2010**, *5*, 556–577.

(15) Suntivich, J.; Gasteiger, H. A.; Yabuuchi, N.; Nakanishi, H.; Goodenough, J. B.; Shao-Horn, Y. Design principles for oxygen-reduction activity on perovskite oxide catalysts for fuel cells and metal–air batteries. *Nature Chem.* **2011**, *3*, 546–550.

(16) Gu, D.; Jia, C.-J.; Weidenthaler, C.; Bongard, H.-J.; Spliethoff, B.; Schmidt, W.; Schüth, F. Highly ordered mesoporous cobalt-containing oxides: structure, catalytic properties, and active sites in oxidation of carbon monoxide. *J. Am. Chem. Soc.* **2015**, *137*, 11407–11418.

(17) Baidya, T.; Murayama, T.; Bera, P.; Safonova, O. V.; Steiger, P.; Katiyar, N. K.; Biswas, K.; Haruta, M. Low-temperature CO oxidation over combustion made Fe-and Cr-doped Co3O4 catalysts: role of dopant's nature toward achieving superior catalytic activity and stability. *J. Phys. Chem. C* **2017**, *121*, 15256–15265.

(18) Royer, S.; Duprez, D. Catalytic oxidation of carbon monoxide over transition metal oxides. *ChemCatChem* **2011**, *3*, 24–65.

(19) Tian, Z.-Y.; Kouotou, P. M.; El Kasmi, A.; Ngamou, P. H. T.; Kohse-Höinghaus, K.; Vieker, H.; Beyer, A.; Gölzhäuser, A. Low-temperature deep oxidation of olefins and DME over cobalt ferrite. *Proceedings of the Combustion Institute* **2015**, *35*, 2207–2214.

(20) Manova, E.; Tsoncheva, T.; Estournes, C.; Paneva, D.; Tenchev, K.; Mitov, I.; Petrov, L. Nanosized iron and iron–cobalt spinel oxides as catalysts for methanol decomposition. *Applied Catalysis A: General* **2006**, *300*, 170–180.

(21) Tong, J.; Bo, L.; Li, Z.; Lei, Z.; Xia, C. Magnetic $CoFe_2O_4$ nanocrystal: A novel and efficient heterogeneous catalyst for aerobic oxidation of cyclohexane. *J. Mol. Catal. A: Chem.* **2009**, *307*, 58–63.

(22) Tan, X.; Wang, X.; Liu, Q.; Zhou, J.; Zhang, P.; Zheng, S.; Miao, S. Bio-gel template synthesis of $CoFe_2O_4$ nano-catalysts and application in aerobic oxidation of cyclohexane. *Int. J. Hydrog. Energy* **2017**, *42*, 19001–19009.

(23) Waffel, D.; Alkan, B.; Fu, Q.; Chen, Y.-T.; Schmidt, S.; Schulz, C.; Wiggers, H.; Muhler, M.; Peng, B. Towards Mechanistic Understanding of Liquid-Phase Cinnamyl Alcohol Oxidation with tert-Butyl Hydroperoxide over Noble-Metal-Free $LaCo_{1--x}Fe_xO_3$ Perovskites. *ChemPlusChem* **2019**, *84*, 1155–1163.

(24) Merino, N. A.; Barbero, B. P.; Ruiz, P.; Cadús, L. E. Synthesis, characterisation, catalytic activity and structural stability of $LaCo_{1-y}Fe_yO_{3\pm\lambda}$ perovskite catalysts for combustion of ethanol and propane. *J. Catal.* **2006**, *240*, 245–257.

(25) Hajiyani, H.; Pentcheva, R. Surface termination and composition control of activity of the $Co_xNi_{1-x}Fe_2O_4(001)$ surface for water oxidation: insights from DFT+ U calculations. *ACS Catal.* **2018**, *8*, 11773–11782.

(26) Chakrapani, K.; Bendt, G.; Hajiyani, H.; Lunkenbein, T.; Greiner, M. T.; Masliuk, L.; Salamon, S.; Landers, J.; Schlögl, R.; Wende, H. et al. The role of composition of uniform and highly dispersed cobalt vanadium iron spinel nanocrystals for oxygen electrocatalysis. *ACS Catal.* **2018**, *8*, 1259–1267.

(27) Waffel, D.; Budiyanto, E.; Porske, T.; Büker, J.; Falk, T.; Fu, Q.; Schmidt, S.; Tüysüz, H.; Muhler, M.; Peng, B. Investigation of Synergistic Effects between Co and Fe in $Co_{3-x}Fe_xO_4$ Spinel Catalysts for the Liquid-Phase Oxidation of Aromatic Alcohols and Styrene. *Mol. Catal.* **2020**, *498*, 111251–9.

(28) Falk, T.; Budiyanto, E.; Dreyer, M.; Pflieger, C.; Waffel, D.; Büker, J.; Weidenthaler, C.; Ortega, K. F.; Behrens, M.; Tüysüz, H. et al. Identification of active sites in the catalytic oxidation of 2-propanol over $Co_{1+x}Fe_{2-x}O_4$ spinel oxides at solid/liquid and solid/gas interfaces. *ChemCatChem* **2021**, *13*, 2942–2951.

(29) Anke, S.; Falk, T.; Bendt, G.; Sinev, I.; Hävecker, M.; Antoni, H.; Zegkinoglou, I.; Jeon, H.; Knop-Gericke, A.; Schlögl, R. et al. On the reversible deactivation of cobalt ferrite spinel nanoparticles applied in selective 2-propanol oxidation. *J. Catal.* **2020**, *382*, 57–68.

(30) Najafishirtari, S.; Ortega, K. F.; Douthwaite, M.; Pattisson, S.; Hutchings, G. J.; Bondue, C. J.; Tschulik, K.; Waffel, D.; Peng, B.; Deitermann, M. et al. A Perspective on Heterogeneous Catalysts for the Selective Oxidation of Alcohols. *Chem. Eur. J.* **2021**, *27*, 16809–16833.

(31) Anke, S.; Bendt, G.; Sinev, I.; Hajiyani, H.; Antoni, H.; Zegkinoglou, I.; Jeon, H.; Pentcheva, R.; Roldan Cuenya, B.; Schulz, S. et al. Selective 2-propanol oxidation over unsupported Co_3O_4 spinel nanoparticles: mechanistic insights into aerobic oxidation of alcohols. *ACS Catal.* **2019**, *9*, 5974–5985.

(32) Ross, J. R. H. *Heterogeneous Catalysis: Fundamentals and Applications*; Elsevier B. V.: Amsterdam, The Netherlands and Oxford, UK, 2012; Chapter 6, pp 123–142.

(33) Rettner, C.; Auerbach, D.; Tully, J.; Kleyn, A. Chemical dynamics at the gas- surface interface. *J. Phys. Chem.* **1996**, *100*, 13021–13033.

(34) Wang, X.; Lan, Z.; Zhang, K.; Chen, J.; Jiang, L.; Wang, R. Structure–Activity Relationships of AMn_2O_4 (A= Cu and Co) Spinels in Selective Catalytic Reduction of NO_x: Experimental and Theoretical Study. *J. Phys. Chem. C* **2017**, *121*, 3339–3349.

(35) Lv, C.-Q.; Liu, C.; Wang, G.-C. A DFT study of methanol oxidation on Co_3O_4. *Catal. Commun.* **2014**, *45*, 83–90.

(36) Rushiti, A.; Hättig, C.; Wen, B.; Selloni, A. Structure and Reactivity of Pristine and Reduced Spinel $CoFe_2O_4$ (001)/(100) Surfaces. *J. Phys. Chem. C* **2021**, *125*, 9774–9781.

(37) Rushiti, A.; Hättig, C. Activation of Molecular O_2 on $CoFe_2O_4$ (001) Surfaces: An Embedded Cluster Study. *Chem. Eur. J.* **2021**, *27*, 17115–17126.

(38) Rushiti, A.; Falk, T.; Muhler, M.; Hättig, C. Interactions of Water and Short-Chain Alcohols with $CoFe_2O_4$ (001) Surfaces at Low Coverages. *Phys. Chem. Chem. Phys.* **2022**, *XX*, 23195–23208.

(39) Zasada, F.; Grybos, J.; Indyka, P.; Piskorz, W.; Kaczmarczyk, J.; Sojka, Z. Surface Structure and Morphology of M[CoM']O_4 (M= Mg, Zn, Fe, Co and M'= Ni, Al, Mn, Co) Spinel Nanocrystals–DFT+ U and TEM Screening Investigations. *J. Phys. Chem. C* **2014**, *118*, 19085–19097.

(40) Burow, A. M.; Sierka, M.; Döbler, J.; Sauer, J. Point defects in CaF_2 and CeO_2 investigated by the periodic electrostatic embedded cluster method. *J. Chem. Phys.* **2009**, *130*, 174710–11.

(41) TURBOMOLE V7.4, 2019, a development of University of Karlsruhe and Forschungszentrum Karlsruhe GmbH, 1989-2007, TURBOMOLE GmbH, since 2007; available from
`http://www.turbomole.com`.

(42) Adamo, C.; Barone, V. Toward reliable density functional methods without adjustable parameters: The PBE0 model. *J. Chem. Phys.* **1999**, *110*, 6158–6170.

(43) Weigend, F.; Ahlrichs, R. Balanced basis sets of split valence, triple zeta valence and quadruple zeta valence quality for H to Rn: Design and assessment of accuracy. *Phys. Chem. Chem. Phys.* **2005**, *7*, 3297–3305.

(44) Burow, A. M.; Sierka, M.; Mohamed, F. Resolution of identity approximation for the Coulomb term in molecular and periodic systems. *J. Chem. Phys.* **2009**, *131*, 214101–6.

(45) Plessow, P. Reaction path optimization without NEB springs or interpolation algorithms. *J. Chem. Theory Comput.* **2013**, *9*, 1305–1310.

(46) Helgaker, T. Transition-state optimizations by trust-region image minimization. *Chem. Phys. Lett.* **1991**, *182*, 503–510.

(47) Høst, S.; Olsen, J.; Jansík, B.; Thøgersen, L.; Jørgensen, P.; Helgaker, T. The augmented Roothaan–Hall method for optimizing Hartree–Fock and Kohn–Sham density matrices. *J. Chem. Phys.* **2008**, *129*, 124106–12.